Functionalizing window coatings with luminescence centers by combinatorial sputtering of scatter-free amorphous SiAlON
Eu^{2+} thin film composition libraries

Merkx, Evert P.J.; van Overbeek, Sadiq; van der Kolk, Erik

DOI
10.1016/j.jlumin.2018.12.011

Publication date
2019

Document Version
Accepted author manuscript

Published in
Journal of Luminescence

Citation (APA)
Merkx, E. P. J., van Overbeek, S., & van der Kolk, E. (2019). Functionalizing window coatings with luminescence centers by combinatorial sputtering of scatter-free amorphous SiAlON: Eu^{2+} thin film composition libraries. *Journal of Luminescence*, *208*, 51-56. https://doi.org/10.1016/j.jlumin.2018.12.011

Functionalizing Window Coatings with Luminescence Centers by Combinatorial Sputtering of Scatter-Free Amorphous SiAlON:Eu^{2+} Thin Film Composition Libraries ¶

Evert P.J. Merkx[a,1,*], Sadiq van Overbeek[b,1], Erik van der Kolk[a]

[a] *Luminescence Materials, Delft University of Technology, Mekelweg 15, 2629 JB, Delft*
[b] *Physee BV, Molengraaffsingel 10, 2629 JD, Delft, the Netherlands*

Abstract

SiAlON window coatings are applied on an industrial scale to achieve e.g. scratch-resistance and anti-reflection. Doping these SiAlONs with rare-earths adds luminescent functionality, which could be applied in photovoltaics. By using a combinatorial reactive sputtering approach, an amorphous thin film composition library with a Si:Al ratio from 0.062 : 1 to 3.375 : 1 and a Eu doping from 4.8 at.% to 26 at.% is created. This library uniquely combines high absorption, strong emission and absence of light scattering. By combining position-dependent EDX measurements with transmission and emission spectra, properties like the index of refraction, absorption strength, emission wavelength and decay times of the library can directly be related to the composition. Throughout the library, an index of refraction of 1.63 ± 0.03 is observed, typical for a film with low nitrogen content. The library also shows a large absorption coefficient of $1294 \pm 8\,\mathrm{cm}^{-1}$ at.%$^{-1}$. Laser-excited emission spectra show that the library has a strong redshift from 500 nm to 550 nm with increasing Al concentration. An increase in Eu concentration also causes a shift of the emission to red. Decay spectra show that a high degree of Si greatly improves the luminescence intensity. These functionalized SiAlON coatings can be of great interest for transparent and scatter-free luminescent solar concentrators applied as windows.

¶DOI: https://doi.org/10.1016/j.jlumin.2018.12.011

*Corresponding author
Email address: e.p.j.merkx@tudelft.nl (Evert P.J. Merkx)
[1]These authors contributed equally to this work.

Highlights

- A large library of unexplored SiAlON:Eu^{2+} compounds is synthesized.
- The SiAlON:Eu thin film library is created using combinatorial reactive sputtering.
- The luminescence color dependence on host composition is characterized, with a higher concentration of Eu or more Al over Si leading to emission shifting from blue to red.
- The compositions in the luminescent thin film library are amorphous and do not scatter light.

1. Introduction

Thin films coatings based on the elements Al, Si, O and N (SiAlON) are applied routinely by the glass industry on a large scale, e.g. for scratch-protection and anti-reflection purposes, because of the coatings' mechanical strength, chemical inertness and thermal resistance[1, 2, 3]. The application range of SiAlON coatings may be expanded by functionalizing them with luminescence centers that can absorb and convert parts of the solar spectrum for electricity generation, utilizing the principle of a luminescent solar concentrator (LSC)[4, 5, 6]. The polycrystalline nature of most luminescent films, however, presents a problem. A polycrystalline material causes light scattering, which lowers applicability for LSCs intended to replace conventional windows. For such a window coating to find broad application, the absence of scattering (haze) in the visible spectrum is a strict requirement. Therefore, scatter-free amorphous luminescent films are desired.

Rare-earth luminescence centers as dopants in SiAlON-based polycrystalline phosphors (also known as SiAlON ceramics) have attracted a great deal of attention for application in white light emitting diodes. In particular, SiAlONs doped with Eu^{2+}, whose emission properties strongly depend on the size and symmetry of the coordinating ions, are actively researched[7, 8, 9, 10, 11]. The SiAlON host provides a wide tuning range of luminescence across the visible spectrum when varying the ratio of Si to Al or the concentration of Eu^{2+}[8]. As a result, a wide range of compositions of polycrystalline SiAlON phosphors exist, where the composition corresponds to emissions ranging from blue to red. Although the wide range of possible SiAlON compositions is beneficial for tuning, exploring all these compositions is time-consuming and challenging.

In this work we present magnetron co-sputtering of Si, Al and Eu in a reactive O_2+N_2+Ar plasma as a technique to explore the luminescence properties of amorphous thin films within a large composition range, requiring only a single deposition. We will show how these SiAlON:Eu^{2+} composition libraries are sputtered and how position-dependent composition is determined through energy dispersive X-ray (EDX) spectroscopy. Following this, position-dependent emission wavelength and intensity, absorption strength, index of refraction and

decay time are determined. Combined with the EDX data, we show how these position-dependent data are converted to ternary diagrams which directly relate composition to the properties of the thin film library. These diagrams allow for a wealth of data to be displayed in a single figure, showing the dependence of a property on three parameters within a single graph. Ternary diagrams are however not often encountered in the field of luminescence. In SiAlON:Eu, these diagrams can show the influence of exchanging cations for each other e.g. Si over Eu, while keeping Al fixed. To read the data in these diagrams, the direction of the axis ticks should be followed. In the Supplementary Information (Figure S3) a more extensive guide can be found.

We will further show that the library spans a composition range that is amorphous, with a haze below 1.1 %, and that the different compositions exhibit emission colors ranging from blue-green to yellow-orange.

2. Experimental

Library creation. The Eu doped SiAlON thin film library was deposited on a square $50 \times 50\,\mathrm{mm}^2$ single crystal MgF_2 substrate within an AJA ATC Orion 5 magnetron sputtering system with a base pressure of 1×10^{-9} bar, at room temperature. Prior to the deposition, the substrate had been cleaned for 15 min in an ultrasonic cleaner with soap solution and had been subsequently rinsed with acetone, ethanol and DI water. The deposition was carried out with 5.08 cm diameter metal Al (99.9995 %, Lesker), Si (99.999 %, Lesker) and Eu (99.99 %, Demaco) targets that were reactively co-sputtered with 75 W DC power, 60 W RF power and 25 W RF power respectively for 11.25 h. The deposition rate of Eu was reduced with a stainless steel mask, with a pattern of concentric holes 5.45 mm in diameter, blocking 60 % of the surface of the Eu target. The process gas flow consisted of 18 sccm 6 N purity Ar, 0.5 sccm 5 N purity O_2 and 13.5 sccm 5 N purity N_2 into the sputtering chamber at a working pressure of 4×10^{-3} mbar. O_2 and N_2 were introduced next to the substrate, while Ar was introduced at the Al source. To realize a gradient thin film, the substrate was sputtered without rotation. Hence, the deposition from each source followed a gradient distribution of the sputtered material on the substrate.

Following the sputter deposition, the library was annealed repeatedly in a Solaris 150 rapid thermal processing (RTP) system to activate the luminescence, while avoiding crystallization. The library underwent one RTP cycle of 60 min at 600 °C, one cycle of 45 min at 650 °C and four cycles of 30 min at 700 °C. The annealing procedure was optimized such that the highest possible PL intensity could be reached before crystallization occurred. The annealing temperatures were reached with a ramp rate of 5 °C/s and the RTP system was flushed with 9 SLM N_2 containing 7 % H_2 (5 N purity) during the entire annealing procedure.

Composition analysis. SEM/EDX analysis was carried out using a JEOL IT-100 operated at 15 keV, with PC 70. Low vacuum mode (35 Pa pressure) was used to facilitate quantitative elemental analysis without a conductive coating.

Elemental compositions were quantified at 1000× magnification. XRD measurements were performed using a PANalytical X'pert Pro MPD diffractometer with a Cu Kα anode ($\lambda = 0.1540598\,\mathrm{nm}$) operating at 45 kV and 40 mA. The area illuminated by the X-ray beam was around $1 \times 5\,\mathrm{mm}^2$ in size.

XY-Scanning technique. A PerkinElmer Lambda 950 UV/VIS spectrophotometer with diffuse reflectance accessory was used to measure haze. The sample was illuminated with a tungsten halogen lamp in the 300 nm to 1300 nm spectral range using a step size of 1 nm. Because of the low degree of haze, transmission measurements were carried out by measuring the direct transmittance. The transmission was measured by placing the film between two 600 µm diameter multimode optical fibers, terminated on either side of the film with an achromatic fiber collimator (74-ACR, Ocean Optics). The top fiber was coupled to a focused deuterium lamp (Acton Research, Model 775) and functioned as an unpolarized light source of 4 mm in diameter. After passing through the sample, the transmitted light was collected by the bottom fiber which led to an Ocean Optics USB4000 CCD Spectrometer. The film was clamped to an optical post placed on top of two stacked Thorlabs DDSM100 linear translation stages. These stages facilitate movement of the film between the fibers. Transmission spectra were recorded at 24×24 positions across the library, at 200 nm to 850 nm with an integration time of 5 ms and averaged 100×.

The sample stage of the XY-scanner was made of the same stages as the transmission set-up. An Ekspla NT230 OPO Laser was used as excitation source, operated at an excitation wavelength of 280 nm. Emission was recorded across 32×32 locations on the substrate, using an Ocean Optics QE65000 CCD Spectrometer with a 325 nm longpass filter to remove reflected laser light. The emission was corrected for the quantum efficiency and non-linearity of the detector. Emission was integrated for 500 ms and averaged 10×. For decay studies, the emission, filtered with a 355 nm longpass filter, passed through an Acton Spect-Pro2300 monochromator, using 2 mm slit width set to let 520 nm (20 nm fwhm resolving power) light through with a 300 grooves/mm grating. The monochromator led to a Hamamatsu R7600U-03 PMT operating at −600 V, with the PMT linked to a CAEN DT5730 Digitizer. Decay traces were collected over 1000 laser pulses. Further details on the operating conditions and procedures of the XY-Scanner can be found in the article by Merkx and van der Kolk [12].

3. Results and Discussion

3.1. Fabrication of the Library

The SiAlON:Eu composition library is fabricated using three elemental sputtering sources (Figure 1a) in a reactive O_2 + N_2 + Ar atmosphere at room temperature. Following deposition, the luminescence of the library is improved by repeated heating in a rapid thermal processor. This treatment leads to a scatter-free thin film, with luminescence clearly visible by the naked eye when excited with UV light (Figure 1b).

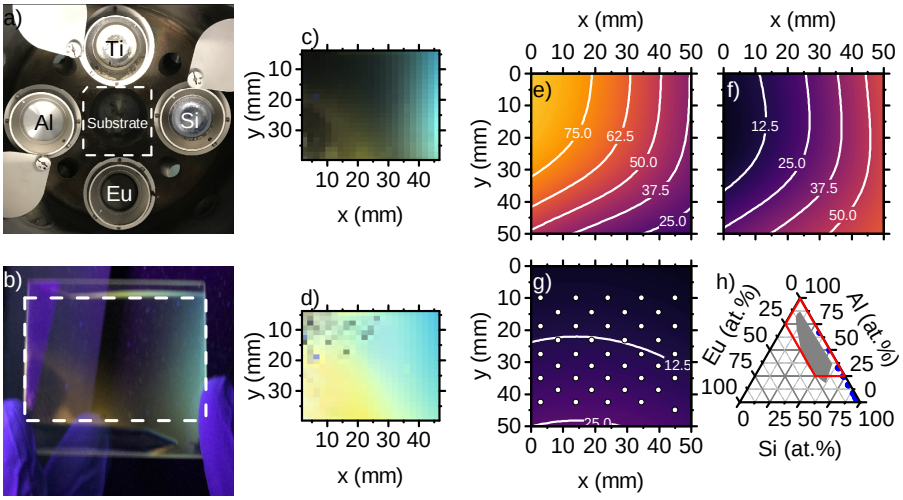

Figure 1: Compositional library of SiAlON doped with Eu. a) Photograph inside of the sputtering system. The Ti source is not used. b) Photograph of the library under UV illumination, after annealing. The triangular cutouts in the film are a result of how the substrate was attached in the sputtering system. The dashed outline indicates the region under investigation. c) RGB color mapping of emission emanating from the library after 280 nm laser excitation. d) RGB mapping of the emission from panel c with normalized emission spectra. Respective distribution of e) aluminum, f) silicon, g) europium across the MgF_2 substrate. Presented data is fit ($R^2 > 0.94$) based on EDX measurements at 40 positions (white dots shown in panel g). The presented percentages are relative to the sum of all cations. h) Ternary overview, here the direction of the axis ticks should be followed to read the data. The gray area is the total composition space present in the library. The red outline shows the cropping which is applied in all following ternary diagrams. Blue dots are compositions previously presented in literature[7, 13, 14, 9, 15, 16, 17, 18, 8, 19].

With a so-called XY-scanner setup[12] a rasterized image of the luminescence is made. Figure 1c shows such an image, obtained by measuring 32×32 individual points of emission across the area of interest (dashed outline in Figure 1b) after local excitation with a tunable OPO laser at 280 nm. To obtain this image, the emission spectra are converted to CIE 1931 xyY coordinates, which in turn are mapped to their respective RGB value. The RGB-based colors shown in Figure 1c closely resemble the photograph of Figure 1b. A clearer view of the color emitted by the library is obtained by normalizing all measured emission spectra, which leads to leaving out luminance information captured by the Y CIE coordinate. These normalized color data are shown in Figure 1d and will be used throughout this article to indicate where on the library measurements were taken.

EDX is carried out on 40 positions across the library (shown in Figure 1g) to determine the local chemical composition. These measurements are interpolated using the surface-source equation[12, 20] to retrieve the continuous composition spread across the library. Si varies from 5 at.% to 62 at.% (Figure 1e), Al from 18 at.% to 87 at.% (Figure 1f) and Eu from 4.8 at.% to 26 at.% (Figure 1g). The curved shapes of EDX mappings are a consequence of the spherical sputtering distribution of the individual sources[12]. At the top ($y < 20$ mm) the shape is mainly dictated by the high sputtering yield of Al. At the bottom ($y > 20$ mm) the combination of the high yields of Eu and Al makes the white iso-concentration lines mainly follow the shape imposed by those two sources. Figure 1h shows a ternary overview of the total compositional space this library spans. As can be seen in Figure 1h, Eu doped SiAlONs with such high Al concentration are not often encountered in literature. SiAlONs richer in Si are more commonly synthesized[7, 14, 19, 9, 16, 17, 18, 21]. Exceptions are the works by Xie et al. [8], Ho Ryu et al. [15] and Zhu et al. [13], where Al:Si ratios as high as 2 : 1 are reported. The library under investigation in this work spans a composition space complimentary to what has been found in the literature cited above. The onset of loss of external quantum efficiency (EQE) is commonly reported at Eu concentrations between 3 at.% and 10 at.% in powdered phosphors[22, 23, 24, 25]. This EQE loss is caused by concentration quenching outweighing absorption. In these powdered phosphors, the incident light is scattered, which causes more absorption than in thin film systems[5]. Therefore, the EQE starts decreasing at higher dopant concentrations in luminescent thin films. Based on this and (unpublished) preliminary observations, our library is deposited with Eu concentrations between 4.8 at.% and 26 at.%. This can be seen as a compromise between absorption and concentration quenching. X-ray diffraction measurements (Figure S1) confirm the amorphous nature of the library.

3.2. Index of Refraction and Absorption

Figure 2a shows the direct transmittance and the amount of haze from the thin film library. The library shows no absorption in the visible range, but strong 4f $\rightarrow$ 5d absorption by Eu^{2+} in the UV. The library exhibits a low degree of haze (the ratio of diffuse to the total transmission) in the visible range, which

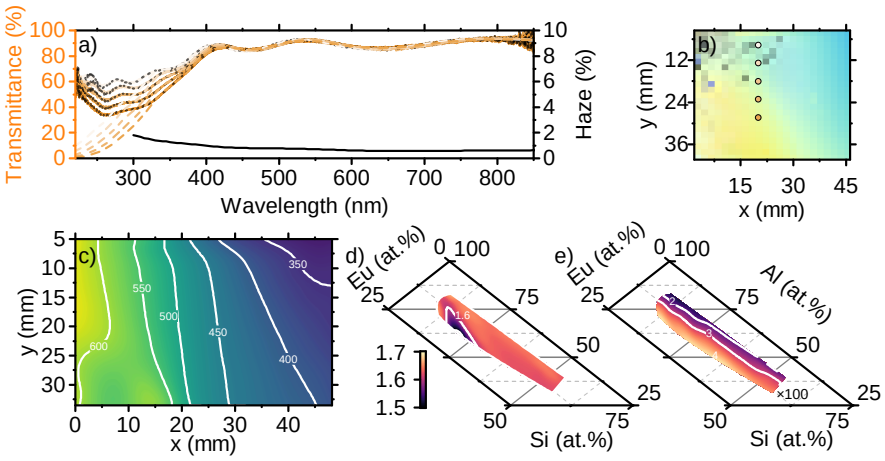

Figure 2: a) Transmittance at locations shown in b). Colored dashed lines are fits to the transmission data ($R^2 = 0.992 \pm 0.005$ for $\lambda > 310\,\text{nm}$), black dotted lines are the fit corrected for Eu-absorption. c) Thickness (in nm) across the film. Respective ternary plots of d) the index of refraction (at 589 nm) and e) the extinction coefficient (at 267 nm, multiplied by a factor 100).

remains below 1.1 %. For comparison, uncoated UV fused silica has a maximal haze of 0.7 %.

The transmission is measured at 24×24 locations across the substrate. The dashed lines in Figure 2a are a fit to the interference fringes and provide the thickness, extinction coefficient and index of refraction n. The fitting procedure and the extended Sellmeier model behind it[26] are explained in detail in the Supplementary Information. It follows that the thickness of the film varies from 322 nm to 639 nm (Figure 2c) as a result of the higher sputter yield of the Al source in comparison to the yields from the Si and Eu sources.

The fitted values for the index of refraction can be combined with the compositional data from Figures 1e to 1g, leading to the ternary diagram as seen in Figure 2d. These ternary diagrams directly relate the composition with other properties, by leaving out position information. Figure 2d shows that the refractive index remains quite constant at $n = 1.63 \pm 0.03$. A minimum of $n = 1.46$ is found at 20 at.% Si, 64 at.% Al and 16 at.% Eu. The index of refraction can assist in clarifying the oxide or nitride nature of the library, which cannot reliably be determined by EDX. Based on the refractive indices of AlN (2.16[27]), Si_3N_4 (2.04[28]), Al_2O_3 (1.76[29, 4-143]) and SiO_2 (1.46[29, 10-249]), we can conclude that the library lies closer to an oxide-type than to a nitride-type material. Within a material, the anions are mainly responsible for the value of n. Since n is constant for most of the library, we can conclude that the O:N ratio within our SiAlONs are the same throughout the library, with only the cations varying. The emergence of the minimum of $n = 1.46$ can however not

be explained, as it greatly deviates from the gradual change of n observed in the rest of the library.

The shape of the UV absorption cannot be described with a monotonically decreasing function as employed by the extended Sellmeier model. However, the model describes the transmission in the range of low absorption very well. It is therefore possible to extrapolate this data to the UV and extract the absorption caused by Eu, expressed as the extinction coefficient, as seen in Figure 2e. Figure 2e shows that the extinction coefficient displays a direct correlation with the doping percentage of Eu, supporting our reasoning that the absorption is caused by Eu. Across the library, this amounts to a (Napierian) attenuation coefficient of $1294 \pm 8\,\mathrm{cm}^{-1}$ at.%$^{-1}$ at the absorption maximum of 267 nm.

3.3. Luminescent Properties

Figure 1d shows that the dominant emission color varies across the SiAlON:Eu library from yellow to blue. The emission observed is a broad band (Figure 3a) attributable to 5d $\rightarrow$ 4f transitions in Eu^{2+}. The wavelength at which the emission is most intense varies from 550 nm at 59.7 at.% Si, 29.9 at.% Al and 10.4 at.% Eu to 500 nm at 82.0 at.% Si, 16.4 at.% Al and 1.6 at.% Eu. This variation corresponds to yellow emission when the library is rich in Al with a shift to blue when the Si concentration is increased. A redshift in emission when the Al:Si ratio increases is often reported in literature for Eu doped SiAlONs[15, 7, 8, 17].

Figures 3a to 3c show that the emission can be deconvoluted into three separate Gaussians. Figure 3a shows all three Gaussians: an intense band, centered at 550 nm, and two bands of lower intensity on both sides of this central band. These three bands change in position and intensity, dependent on the composition of the library. The band at higher wavelengths starts to become discernible when starting at the right (Si-rich side) of the library and moving to a decreasing Si concentration (Figure 3b), with measurement positions shown in the inset of Figure 3a. The band at lower wavelengths becomes clearly visible at higher Eu and Al concentrations (bottom left of the library, as seen in the inset).

The three bands are fit to the spectra of all emission measurements. The fitting protocol is similar to that for the transmission measurements, explained in the Supplementary Information. A limitation is placed on how much the width (fwhm) of each band is allowed to vary across the library. This limitation asserts that the bands have the same physical origin in the host lattice, as opposed to producing the numerically best fit. This yields a variation of 0.73 ± 0.06 eV fwhm for the band at low wavelengths, 0.64 ± 0.07 eV fwhm for the center band, and 0.67 ± 0.05 eV fwhm for the band at high wavelengths. The center attributed to a band is allowed to vary by at most 0.05 eV per step in position ($\Delta x = 1.72$ mm, $\Delta y = 1.89$ mm). This limitation asserts that the gradual shifting of composition is reflected in the fitting of the emission. No limitations are placed on the maximal or minimal intensity of the bands.

The amorphous nature complicates a discussion of the origin of the luminescent properties derived from the material's crystal structure. However, the

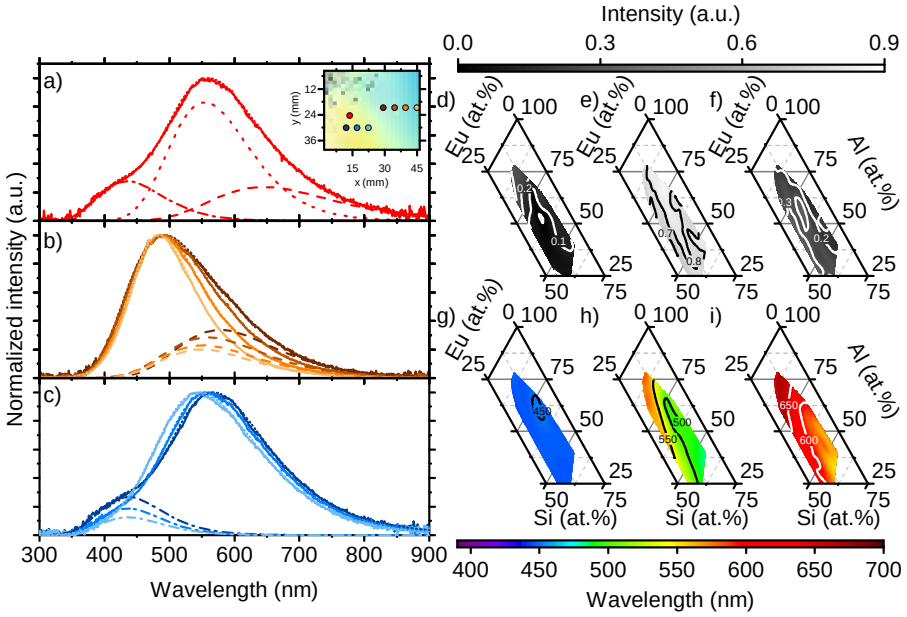

Figure 3: Relation between composition and luminescent emission ($\lambda_{ex} = 280\,nm$) properties of the library. a) Emission spectrum observed at the red point in the inset, showing the three different Gaussians that build up the observed emission. The measured emission is a solid line, fits are dotted. b) Normalized emission spectra (yellow-to-brown points shown in the inset of panel a) showing the development of the band at high wavelengths (dashed), while the center and low wavelength bands remain constant. c) Normalized emission spectra where the presence of the band at low wavelengths (dash-dotted) becomes visible (light-to-dark blue points in the inset of panel a). Ternary diagrams of the deconvoluted intensities of the normalized spectra for d) the low-wavelength band, e) the center band, f) the high wavelength band. Centers (in nm) of these bands are respectively shown in g),h),i) (adjusted-$R^2 > 0.99$).

widths of the different emissions show limited variation while still producing a good fit. We can therefore conclude that the observed emissions originate from three defects for which the first coordination sphere does not change throughout the library. This corresponds with the constant index of refraction throughout the library, further establishing that the O:N ratio in the library is constant to a great degree.

Like the data resultant from the fitting of the transmissions, the properties of the Gaussians can also be directly related to the composition. Figures 3d to 3f show ternary diagrams for the emission intensities and Figures 3g to 3i for the center wavelengths of the three deconvoluted Gaussians.

Comparing the ternary intensity diagrams shows that the central band (at $\sim 500 - 550\,\mathrm{nm}$) is most intense throughout the entire library. This central band is therefore mainly responsible for the observed emission color. The band at low wavelengths (Figures 3d and 3g) becomes relatively more intense at higher Al concentrations, while the intensities of the other two bands show no clear correlation with the composition.

From the ternary emission diagrams (Figures 3g to 3i), the influence of substituting the cations in SiAlON:Eu for each other becomes immediately visible. For the two emissions at higher wavelengths (Figures 3h and 3i), a shift of the emission to the red can be observed when (*i*) substituting Si for Al at a fixed Eu concentration, and (*ii*) increasing the Eu concentration, where Eu substitutes either Si or Al.

In the case of (*i*), a change in the second coordination sphere surrounding the emitting Eu can explain the increasing emission wavelengths. In this second coordination sphere, the distribution of Al and Si cations can be assumed to vary statistically, based on the measured composition. Since Al has a lower electronegativity than Si, it tends to bind the electrons of the neighboring anion less strongly. Consequently, the anions in the first coordination sphere of Eu^{2+} become more polarizable (i.e. have a higher spectroscopic polarizability[30].) This increase in polarizability leads to a decrease in centroid energy[30] (difference between the 4f groundstate and average 5d-level) when the Al concentration increases, and thus to a higher emission wavelength. This same effect of redshifting emission when replacing Si with Al in the second coordination sphere has been observed in Tb^{3+} doped $Y_2Ca_2Si_2O_9$ and $Y_4Al_2O_9$[31].

The redshift related to an increased Eu concentration (*ii*) can be caused by reabsorption of the high-energy shoulder of the emission. This reabsorption effect becomes more profound with more absorbing centers present and will therefore yield a phosphor emitting at low energy and thus high wavelength[32].

Contrary to the other two emissions, the band at lower wavelength (Figure 3g) remains at a relatively constant wavelength, moving from 444 nm to 452 nm. A blue-violet emission in Al-rich SiAlONs has been previously reported in literature by Zhu et al. [13] and Yang et al. [16] It appears that this defect is located at a site where the emission is unaffected by changes in overall host composition. The relative intensity of this emission does however start increasing when the concentration of Al is increased (Figure 3d), as is also observed by Zhu et al. [13] This blue-violet emission has been attributed to a defect site

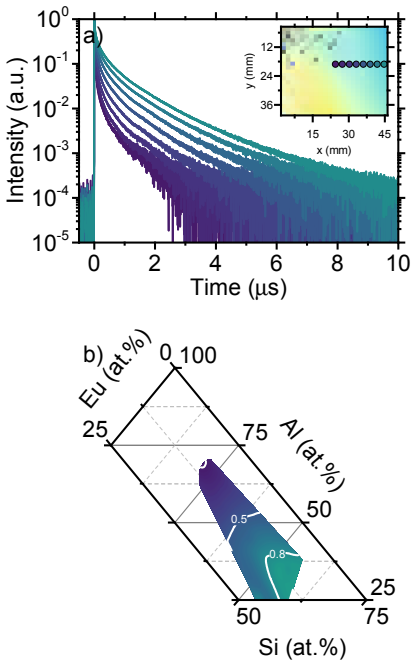

Figure 4: Decay times across the substrate (λ_{ex} = 280 nm, λ_{em} = 510 nm to 530 nm). a) Moving from the locations rich in Si to rich in Al at equal Eu (see inset). b) Ternary plot of mean decay times (in µs).

with higher oxygen content in its first coordination sphere than defects showing emission at higher wavelengths[13]. This higher oxygen content should go paired with a lower index of refraction. Figure 2d confirms that this is indeed the case, as a lower n is observed at higher Al concentrations, where this defect becomes visible.

3.4. Luminescent Quantum Efficiency

The photoluminescent (PL) intensity (Figure 1c) varies strongly as a function of position and hence composition. Since the thickness and amount of dopant vary throughout the film, the PL is not a direct measure for the efficiency with which the dopants convert the absorbed light [i.e. the luminescent quantum efficiency (LQE)]. A measure for the LQE independent of all these parameters is the decay time, which only depends on properties of the composition itself.

Figure 4a shows that the photoluminescent decay of the library after excitation at 280 nm is strongly non-exponential. Therefore, the decay time cannot be fitted with a single exponent, which would yield the decay time. To still have a comparative measure, a mean decay time[33]

$$\tau_{\text{mean}} = \frac{\int_0^\infty tI(t)\,\mathrm{d}t}{\int_0^\infty I(t)\,\mathrm{d}t} \tag{1}$$

is calculated. Here, $I(t)$ is the emission intensity at time t after excitation.

Figure 4b shows the mean decay times summarized in a ternary diagram. The quantum efficiency can be estimated by comparing τ_{mean} to an ideal decay time of an isolated emitting center. Assuming that this ideal decay time does not vary greatly across the different compositions, τ_{mean} can be taken as a relative estimate of the LQE. Figure 4b shows that an increase in Si concentration over Al leads to an increase in τ_{mean}. Combined with the higher PL intensity seen in Figure 1c, we can therefore conclude that when increasing the Si concentration, also the quantum efficiency increases. This increasing quantum efficiency with higher Si concentrations agrees with what is observed in literature, where for crystalline Eu doped β-SiAlON the highest quantum efficiencies were found for a Si:Al ratio greater than 5 : 1, with decreasing quantum efficiency as this ratio decreases[8].

The decrease in decay time for decreasing Si content over Al might be related to two different effects. As the Si:Al ratio decreases, the distance between all atoms increases and the overall structure becomes less rigid[8, 11]. This can yield a smaller radial overlap between the 4f and 5d orbitals of Eu^{2+}, which has a decreased decay time as a consequence[34]. Another possibility is that the decrease in decay time comes from a decrease in thermal stability as the Si:Al ratio decreases. As the 5d energy level lowers towards the 4f level, the parabolas describing the two in a configurational coordinate diagram will intersect at lower energy. Physically, this means a higher likelihood of a radiationless transition at room temperature, which goes paired with a lower decay time.

4. Conclusion

We have shown that it is possible to create an amorphous luminescent thin film material-library with a specific Al:Si:Eu composition range in a SiAlON host, with a haze below 1.1 % in the visible spectrum and strong PL emission. The library shows clear composition-dependent emission varying from 500 nm to 550 nm after UV excitation. An increase in Al concentration over Si goes together with an increase in emission wavelength. This behavior can be best explained by that the composition of the second coordination sphere of the dominant Eu defect shifts the emission to the red. Simultaneously with shifting the emission to the red, the quantum efficiency drops. We can therefore conclude that a higher degree of Si in our SiAlON:Eu^{2+} thin film improves the quantum efficiency of the Eu^{2+} emission.

The low haze combined with the amorphous nature of the library opens up possibilities for functionalizing sputter deposited luminescent SiAlONs as a luminescent solar concentrator. The Eu doping shown in this article only absorbs the UV portion of sunlight, which could make for a visibly transparent luminescent solar concentrator with low power output. However, using the

same methods of library creation with sputter coating and subsequent analysis, other rare-earths, like Sm^{2+} and Tm^{2+}, can be doped into similar amorphous SiAlON hosts. These rare-earths could expand the absorption range to span the visible range and therefore greatly increase the total achievable solar-to-electric conversion efficiency.

5. Acknowledgements

The authors would like to acknowledge Rudi Santbergen for assisting with the haze measurements. EM and SO contributed equally to this work. This work was supported by the Netherlands Organization for Scientific Research (NWO/OCW), as part of the Frontiers of Nanoscience program (NF16NFS01) and as part of the LumiCon project (15024).

References

[1] R.-J. Xie, H. T. Bert Hintzen, Optical Properties of (Oxy)Nitride Materials: A Review, Journal of the American Ceramic Society 96 (2013) 665–687.

[2] G. Bernhardt, J. Krassikoff, B. Sturtevant, R. Lad, Properties of amorphous SiAlON thin films grown by RF magnetron co-sputtering, Surface and Coatings Technology 258 (2014) 1191–1195.

[3] T. Ekstrom, M. Nygren, SiAlON Ceramics, Journal of the American Ceramic Society 75 (1992) 259–276.

[4] W. H. Weber, J. Lambe, Luminescent greenhouse collector for solar radiation., Applied Optics 15 (1976) 2299–2300.

[5] D. K. G. de Boer, D. J. Broer, M. G. Debije, W. Keur, A. Meijerink, C. R. Ronda, P. P. C. Verbunt, Progress in phosphors and filters for luminescent solar concentrators., Optics Express 20 (2012) A395–405.

[6] M. Debije, Renewable energy: Better luminescent solar panels in prospect, Nature 519 (2015) 298–299.

[7] C. Cozzan, G. Laurita, M. W. Gaultois, M. Cohen, A. A. Mikhailovsky, M. Balasubramanian, R. Seshadri, Understanding the links between composition, polyhedral distortion, and luminescence properties in green-emitting β-$Si_{6-z}Al_zO_zN_{8-z}$:Eu^{2+} phosphors, Journal of Materials Chemistry C 5 (2017) 10039–10046.

[8] R.-J. Xie, N. Hirosaki, H.-L. Li, Y. Q. Li, M. Mitomo, Synthesis and Photoluminescence Properties of β-sialon:Eu^{2+} ($Si_{6-z}Al_zO_zN_{8-z}$:Eu^{2+}), Journal of The Electrochemical Society 154 (2007) J314.

[9] N. Hirosaki, R.-J. Xie, K. Kimoto, T. Sekiguchi, Y. Yamamoto, T. Suehiro, M. Mitomo, Characterization and properties of green-emitting β-SiAlON:Eu^{2+} powder phosphors for white light-emitting diodes, Applied Physics Letters 86 (2005) 211905.

[10] R.-J. Xie, N. Hirosaki, Silicon-based oxynitride and nitride phosphors for white LEDs–A review, Science and Technology of Advanced Materials 8 (2007) 588–600.

[11] X. Zhang, M.-H. Fang, Y.-T. Tsai, A. Lazarowska, S. Mahlik, T. Lesniewski, M. Grinberg, W. K. Pang, F. Pan, C. Liang, W. Zhou, J. Wang, J.-F. Lee, B.-M. Cheng, T.-L. Hung, Y.-Y. Chen, R.-S. Liu, Controlling of Structural Ordering and Rigidity of β-SiAlON:Eu through Chemical Cosubstitution to Approach Narrow-Band-Emission for Light-Emitting Diodes Application, Chemistry of Materials 29 (2017) 6781–6792.

[12] E. P. J. Merkx, E. van der Kolk, Method for the Detailed Characterization of Cosputtered Inorganic Luminescent Material Libraries, ACS Combinatorial Science (2018) acscombsci.8b00068.

[13] X. W. Zhu, Y. Masubuchi, T. Motohashi, S. Kikkawa, The z value dependence of photoluminescence in Eu^{2+}-doped β-SiAlON ($Si_{6-z}Al_zO_zN_{8-z}$) with $1 \leq z \leq 4$, Journal of Alloys and Compounds 489 (2010) 157–161.

[14] C.-Y. Chung, J. H. Ryu, D. S. Yoo, S.-H. Lee, Y.-C. Chung, First-principles calculation and luminescence property of Eu_x:$Si_5Al_{1-x}O_{1+x}N_{7-x}$ green phosphor, Computational Materials Science 49 (2010) S359–S363.

[15] J. Ho Ryu, Y.-G. Park, H. Sik Won, S. Hyun Kim, H. Suzuki, C. Yoon, Luminescence properties of Eu^{2+}-doped β-$Si_{6-z}Al_zO_zN_{8-z}$ microcrystals fabricated by gas pressured reaction, Journal of Crystal Growth 311 (2009) 878–882.

[16] H. Yang, Q. Liu, Q. Wei, Z. Zhou, J. Wan, G. Liu, R.-J. Xie, Eu-Doped β-SiAlON Phosphors: Template-Assistant Low Temperature Synthesis, Dual Band Emission, and High-Thermal Stability, Journal of the American Ceramic Society 97 (2014) 3164–3169.

[17] Y. Li, N. Hirosaki, R. Xie, T. Takeda, M. Mitomo, Crystal and electronic structures, luminescence properties of Eu^{2+}-doped $Si_{6-z}Al_zO_zN_{8-z}$ and $M_ySi_{6-z}Al_{z-y}O_{z+y}N_{8-z-y}$ (M=2 Li, Mg, Ca, Sr, Ba), Journal of Solid State Chemistry 181 (2008) 3200–3210.

[18] T. Wang, Z. Xia, Q. Xiang, S. Qin, Q. Liu, Relationship of 5d-level energies of Ce^{3+} with the structure and composition of nitride hosts, Journal of Luminescence 166 (2015) 106–110.

[19] J. H. Chung, J. H. Ryu, Photoluminescence and LED application of b−SiAlON:Eu^{2+} green phosphor, Ceramics International 38 (2012) 4601–4606.

[20] J. D. Fowlkes, J. M. Fitz-Gerald, P. D. Rack, Ultraviolet emitting $(Y_{1-x}Gd_x)_2O_{3-\delta}$ thin films deposited by radio frequency magnetron sputtering: Combinatorial modeling, synthesis, and rapid characterization, Thin Solid Films 510 (2006) 68–76.

[21] S. Yamada, H. Emoto, M. Ibukiyama, N. Hirosaki, Properties of SiAlON powder phosphors for white LEDs, Journal of the European Ceramic Society 32 (2012) 1355–1358.

[22] S. W. Kim, T. Hasegawa, T. Ishigaki, K. Uematsu, K. Toda, M. Sato, Efficient Red Emission of Blue-Light Excitable New Structure Type $NaMgPO_4$:Eu^{2+} Phosphor, ECS Solid State Letters 2 (2013) R49–R51.

[23] C. Zhang, J. Yang, C. Lin, C. Li, J. Lin, Reduction of Eu^{3+} to Eu^{2+} in $MAl_2Si_2O_8$ (M=Ca, Sr, Ba) in air condition, Journal of Solid State Chemistry 182 (2009) 1673–1678.

[24] X. Qiao, H. J. Seo, A Novel Blue-Emitting Phosphor of Eu^{2+}-Activated Magnesium Haloborate $Mg_3B_7O_{13}Cl$, Journal of the American Ceramic Society 98 (2015) 594–600.

[25] T.-W. Kuo, C.-H. Huang, T.-M. Chen, Novel yellowish-orange $Sr_8Al_{12}O_{24}S_2$:Eu^{2+} phosphor for application in blue light-emitting diode based white LED, Optics Express 18 (2010) A231.

[26] R. Alvarez, A. Garcia-Valenzuela, C. Lopez-Santos, F. J. Ferrer, V. Rico, E. Guillen, M. Alcon-Camas, R. Escobar-Galindo, A. R. Gonzalez-Elipe, A. Palmero, High-Rate Deposition of Stoichiometric Compounds by Reactive Magnetron Sputtering at Oblique Angles, Plasma Processes and Polymers 13 (2016) 960–964.

[27] S. Adachi, Optical Constants of Crystalline and Amorphous Semiconductors: Numerical Data and Graphical Information, Springer US, Boston, MA, 1999. URL: http://link.springer.com/10.1007/978-1-4615-5247-5. doi:10.1007/978-1-4615-5247-5.

[28] K. Luke, Y. Okawachi, M. R. E. Lamont, A. L. Gaeta, M. Lipson, Broadband mid-infrared frequency comb generation in a Si_3N_4 microresonator, Optics Letters 40 (2015) 4823.

[29] D. R. Lide, CRC Handbook of Chemistry and Physics, 2007. doi:10.4324/9781410610348.

[30] P. Dorenbos, 5d-level energies of Ce^{3+} and the crystalline environment. I. Fluoride compounds, Physical Review B 62 (2000) 640–649.

[31] G. Blasse, A. Bril, Investigations of Tb^{3+}-activated phosphors, Philips Research Reports 22 (1967) 481–502.

[32] C.-Y. Wang, T. Takeda, O. M. ten Kate, R.-J. Xie, K. Takahashi, N. Hirosaki, Synthesis and photoluminescence properties of a phase pure green-emitting eu doped jem sialon ($LaSi_{6-z}Al_{1+z}N_{10-z}O_z$, $z \sim 1$) phosphor with a large red-shift of emission and unusual thermal quenching behavior, Journal of Materials Chemistry C 4 (2016) 10358–10366.

[33] E. Nakazawa, Fundamentals of luminescence, in: W. M. Yen, S. Shionoya, H. Yamamoto (Eds.), Phosphor Handbook, 2 ed., CRC Press, 2006, pp. 99–110.

[34] S. Poort, A. Meyerink, G. Blasse, Lifetime measurements in Eu^{2+}-doped host lattices, Journal of Physics and Chemistry of Solids 58 (1997) 1451–1456.